Z. Angew. Math. Phys. (2026) 77:1

https://doi.org/10.1007/s00033-025-02626-3

Zeitschrift für angewandte Mathematik und Physik ZAMP

On the hard loss of stability of the Beck's beam

G. Migliaccio, A. Casalotti and F. D'Annibale

Abstract. This paper investigates the complex nonlinear dynamics of non-conservative mechanical systems under different sources of nonlinear damping, including internal damping from material behavior and external damping due to fluid–structure interactions. A Beck's beam, namely, a viscoelastic cantilever beam subjected to a follower force at its free end, is taken as a paradigmatic example. The governing equations of motion are derived using a variational principle, then reformulated into an integro-differential form and discretized through the Galerkin method. Starting from the Hopf bifurcation, identified via the linear stability analysis, the nonlinear post-critical behavior of the discretized system close to it is analyzed using the Multiple Scales Method. This perturbation technique yields bifurcation equations whose analysis reveals new aspects of damping-induced destabilization, including the dual nature of nonlinear damping, which can either promote stability or induce instability in the bifurcated response of the system, as well as the emergence of the so-called Hard Loss of Stability phenomenon, analytically predicted by a second-order amplitude modulation equation. Numerical analyses are finally performed and corroborate the analytical findings of the study.

Mathematics Subject Classification. 70H14, 70H25, 70J25, 70Q05, 74K10.

Keywords. Nonlinear dynamics, Hard loss of stability, Multiple Scales Method.

1. Introduction

The study of the nonlinear dynamics and stability of non-conservative mechanical systems is a foundational topic in solid and structural mechanics [1–5]. This enduring area of research continues to captivate contemporary engineers and scientists due to its critical role in a broad spectrum of advanced technologies. Key areas of investigation include jet- and rocket-propelled aerospace vehicles [6–9], elastic systems affected by dry friction [10–12], fluid–structure interaction phenomena [13–15], and piezoelectric beams employed in advanced vibration control and energy harvesting applications [16–19], among others.

Instability phenomena frequently encountered in non-conservative systems include divergence and flutter. These phenomena are characteristic of aeroelastic systems, such as aircraft wings, due to the intricate interaction between aerodynamic forces, structural elasticity, and inertial effects. When exposed to high-speed airflow, a wing may exhibit a dynamic response involving coupled bending and torsional modes. This coupling may lead to an exponentially growing bending-twisting motion of the wing when the aerodynamic forces exceed the wing's structural stiffness (divergence), or to oscillatory bending-twisting motions of growing amplitude (flutter), also known as Hopf bifurcation. In structural mechanics, divergence and flutter instabilities are exemplified by several discrete and continuous systems. A classical example of a discrete system is Ziegler's double pendulum, a viscoelastic double pendulum subjected to a follower load [5,20,21]. Its continuous viscoelastic counterpart is represented by the Beck's beam [4,22,23], another foundational model that exhibits similar instability phenomena.

The introduction of damping, whether internal or external, into non-conservative mechanical systems can lead to unexpected dynamic responses [22–30]. Often, damping is external, for example, arising from interaction with an ambient fluid [31]. However, damping can also be internal, caused by material

Published online: 13 December 2025

dissipation mechanisms such as those described by the rheological Kelvin–Voigt model [26,32,33]. The influence of both types of damping sources on the stability of non-conservative systems, such as those subjected to follower loads [10,24,34], can contradict intuitive expectations. In the linear field, it is well-established that introducing even a small amount of internal damping can cause a finite decrease in the critical load of the system compared to the undamped case. This counterintuitive phenomenon is known as Ziegler's paradox [5], or damping destabilization paradox [20,26–28]. Furthermore, detrimental effects of damping have also been observed in the nonlinear regime. For example, in the generalized Beck's beam analyzed in [23], where both dead and follower loads are applied at the free end of a cantilever, nonlinear damping originating from both internal and external sources can increase the amplitude of the system's limit cycles and can even convert a stable supercritical limit cycle into an unstable subcritical one. This highlights a damping-induced destabilizing effect occurring within the nonlinear regime, extending beyond the well-established destabilization effect observed in the linear case [4,22,22,29,30,35].

The mechanical behavior of both discrete and continuous systems influenced by internal and external damping has been extensively examined in the literature. The nonlinear dynamics of Beck's beam under lateral excitation and support motion are explored in [36,37]. Instabilities such as flutter and divergence in vertical columns subjected to follower forces like those generated by jet engines are investigated in [38,39]. Similar follower forces can also arise from dry friction, as discussed in [10,40,41], where both theoretical and experimental studies examine how dry friction can trigger stability loss in slender elastic elements. Critical and post-critical bifurcation scenarios in a Beck's beam are studied using the Method of Multiple Scales in [30,42], revealing divergence, Hopf, and double-zero bifurcations. The stability of a Beck's beam under linear damping and piezoelectric devices has been explored in [43–47]. The nonlinear dynamics near a Hopf bifurcation and the so-called Hard Loss of Stability phenomenon have been investigated in both Beck's beam [22] and Ziegler's double pendulum [21]. Specifically, the Hard Loss of Stability was first discovered in [22] for Beck's beam and later analyzed analytically for Ziegler's double pendulum in [21] in the presence of a Van der Pol-type internal damping. This phenomenon involves the subcritical periodic branch bending back and regaining stability. As a result, immediately after the critical load is surpassed, a large-amplitude limit cycle appears abruptly, without approaching zero at the bifurcation point. A detailed investigation of the nonlinear dynamic behavior of a Beck's beam subjected to both conservative and non-conservative loads, and influenced by internal and external nonlinear damping, is presented in [23] using the Method of Multiple Scales. This study reveals a novel damping-induced destabilization mechanism that goes beyond the well-known destabilizing effects observed in the linear regime [4,22,30]. Moreover, the Hard Loss of Stability is identified numerically in the same system, under the combined influence of internal and external nonlinear damping.

The present paper is framed in the above-mentioned scenario and aims to shed light on the role played by various internal and external nonlinear damping mechanisms in the nonlinear dynamics of a Beck's beam. A fundamental objective is to achieve an analytical identification of the Hard Loss of Stability phenomenon, which, for a Beck's beam, has so far been observed only through numerical simulations. The governing equations of motion are derived using a variational principle, then reformulated into an integro-differential form and discretized through the Galerkin method [48,49]. Starting from Hopf bifurcation points identified via linear stability analysis, the nonlinear post-critical behavior of the discretized system in the vicinity of these bifurcation points is analyzed using the Multiple Scales Method [50,51]. In addition to the damping-induced destabilization effect originally identified in the nonlinear regime in [23], the application of the perturbation technique in the present study yields bifurcation equations that enable the analytical prediction of the Hard Loss of Stability phenomenon. This behavior is characterized by a turning point in the amplitude–load bifurcation diagram, which leads to the restabilization of previously subcritical branches. Finally, numerical analyses are conducted to validate and corroborate the analytical results presented in this work.

The structure of the paper is as follows. Section 2 recalls the mechanical model of the system. In Sect. 4, an asymptotic analysis based on the Method of Multiple Scales is carried out to analytically identify the

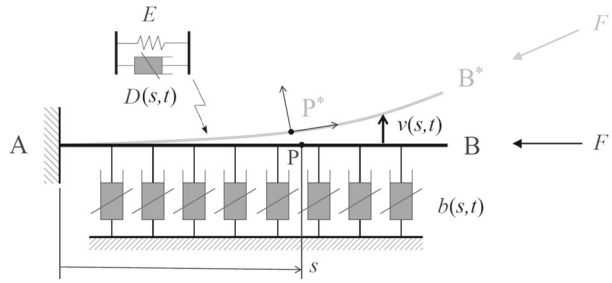

FIG. 1. Reference (black) and deformed (gray) configurations of the viscoelastic beam, with indication of transverse displacement of the beam axis $v(s,t)$, follower load F, Young's modulus of the material E, internal damping function $D(s,t)$, and external damping function $b(s,t)$

system's limit cycles and assess the influence of damping, whether stabilizing or destabilizing, on their behavior, including the occurrence of the Hard Loss of Stability phenomenon. Section 5 validates the analytical predictions through comparison with benchmark numerical results. Finally, Sect. 6 summarizes the main findings and outlines potential directions for future research.

2. Mechanical model

The Beck's beam represented in Fig. 1 is an unshearable, inextensible cantilever beam, made of a nonlinear viscoelastic material. The variable $s \in [0, l]$ is the curvilinear abscissa along the beam's axis of length l, $t \in [0, +\infty)$ is the time variable. Interactions of the beam with the external environment are modeled by a follower non-conservative force, F, applied at the free-end B, plus transverse nonlinear dashpots, distributed along the beam's axis and modeled by the nonlinear external damping function $b(s,t)$.

Following [23] to which the reader is referred for details, the equations of motion of the considered planar beam, governing the horizontal and vertical displacements, $u(s,t)$ and $v(s,t)$, respectively, of the beam's axis, and the rotation $\theta(s,t)$ of the beam's cross sections, are derived using the extended Hamilton's principle (see also "Appendix A") and are recast in the form of a single nonlinear integro-differential equation, which reads

$$-m\ddot{v}(s,t) + p(s,t) + \left[\frac{v'(s,t)\big(H(l,t) - \int_s^l m\ddot{u}(x,t)\big) - M'(s,t)}{1+u'(s,t)}\right]' = 0, \tag{1}$$

where the overdot and prime symbols denote differentiation with respect to the time variable t and axial coordinate s, respectively, m is the mass per unit length of the beam, $M(s,t)$ is the internal bending moment at the cross section s at the time t, $H(l,t) = -F\cos(\theta(l,t))$ is the horizontal component of the tip force in the beam deformed configuration, $p(s,t)$ represents the external action distributed along the beam's axis.

The constitutive law for the bending moment $M(s,t)$ is assumed to be ruled by the following nonlinear viscoelastic model

$$M(s,t) = EI\,\kappa(s,t) + D(s,t)I\,\dot{\kappa}(s,t), \tag{2}$$

where EI is the constant bending stiffness of the beam and $D(s,t)$ is the nonlinear internal damping function defined by

$$D(s,t) = d_0 + d_1\kappa^2(s,t) + d_2\dot{\kappa}^2(s,t), \tag{3}$$

with d_0, d_1, d_2 prescribed constants.

The distributed external load $p(s,t)$ is expressed in the form

$$p(s,t) = -b(s,t)\,\dot{v}(s,t), \tag{4}$$

where $b(s,t)$ is the nonlinear external damping function given by

$$b(s,t) = b_0 + b_1 v^2(s,t) + b_2\dot{v}^2(s,t), \tag{5}$$

with b_0, b_1, b_2 prescribed constants.

Equation (1) is also supplemented by *geometric* boundary conditions imposed at the built-in end ($s = 0$), specifically, $v(0,t) = 0$ and $v'(0,t) = 0$. Additionally, it is complemented by the *natural* boundary conditions $M(l,t) = 0$ and $M'(l,t) = 0$, which are associated with the presence of only a follower load at the free end ($s = l$).

In the following, the dependence of all functions on the independent variables s and t is understood and, hence, omitted. Moreover, equations and variables are put into a dimensionless form by rescaling the time variable t with the time parameter $\tau = \sqrt{ml^4/EI}$ (i.e., $\tilde{t} = t/\tau$), and the spatial variables, s, $v(s,t)$, and $u(s,t)$, with the beam reference length l (i.e., $\tilde{s} = s/l$, $\tilde{v} = v/l$, $\tilde{u} = u/l$).

The system's behavior near a Hopf bifurcation, i.e., in the so-called post-critical regime, will be analyzed, with particular attention given to the influence of nonlinear damping on its dynamics. To this end, the model equations are expanded in a Taylor series up to cubic terms and reformulated in a non-dimensional form, as follows,

$$\begin{cases} \ddot{v} + v'''' + 2\mu v'' + \alpha_0\dot{v}'''' + \beta_0\dot{v} + \alpha_1(\dot{v}''v''^2)'' + \beta_1\dot{v}v^2 + f = 0, \\ v''_B + \alpha_0\dot{v}''_B + \alpha_1\dot{v}''_B v''^2_B + g_B = 0, \\ v'''_B + \alpha_0\dot{v}'''_B + \alpha_1(\dot{v}''_B v''^2_B)' + g'_B = 0, \\ v_A = 0, \\ v'_A = 0, \end{cases} \tag{6}$$

where prime and dot denote differentiation with respect to non-dimensional abscissa s and time t (*tilde* is omitted), respectively, subscript A (B) denotes evaluation of functions at the abscissa $s = 0$ ($s = 1$), $\mu = \frac{F\,l^2}{2EI}$ represents the non-dimensional follower load, $\alpha_0 = \frac{d_0\,I}{EI\,\tilde{t}}$ and $\beta_0 = \frac{b_0 l^4}{EI\,\tilde{t}}$ are the linear damping parameters of the internal and external type, $\alpha_1 = \frac{d_1\,I}{EI\,l^2\,\tilde{t}}$ and $\beta_1 = \frac{b_1 l^5}{EI\,\tilde{t}}$ are the nonlinear damping parameters of the internal and external type, and, finally,

$$f = [v'(v'v'')']' + \alpha_0\{[v'(v'v'')']'\}^{\cdot} + \left[v'\int_1^s\int_0^{s^*}\dot{v}'\dot{v}' + v'\ddot{v}'\right]' + \mu v''(3v'^2 - v'^2_B), \tag{7}$$

$$g = \frac{v'^2 v'' + \alpha_0(v'^2 v'')^{\cdot}}{2}. \tag{8}$$

2.1. Discretization approach

Before introducing the perturbation approach adopted in this work to analytically investigate the influence of nonlinear damping on the system's post-critical behavior, Eq. (6) is first discretized using the Galerkin method. In this framework, the displacement is expressed as $\sum_{k=1}^{n_m} \phi_k(s) q_k(t)$, where n_m are the number of modes retained, q_k are the generalized coordinates, and ϕ_k are the trial functions. These latter are chosen as the eigenfunctions of the linear, undamped ($\alpha_0 = \beta_0 = 0$), free-vibration ($\mu = 0$) problem of a cantilever beam, namely,

$$\begin{cases} \phi_k'''' - \sigma_k^4 \phi_k = 0, \\ \phi_k''(1) = \phi_k'''(1) = 0, \\ \phi_k(0) = \phi_k'(0) = 0, \end{cases} \tag{9}$$

and are normalized according to the condition

$$\int_0^1 \phi_k(s)\phi_j(s)\mathrm{d}s = \delta_{kj}, \tag{10}$$

where δ_{kj} is the Kronecker's delta. Consequently,

$$\phi_k(s) = \cos(\sigma_k s) - \cosh(\sigma_k s) - \frac{\cos(\sigma_k) + \cosh(\sigma_k)}{\sin(\sigma_k) + \sinh(\sigma_k)}(\sin(\sigma_k s) - \sinh(\sigma_k s)), \tag{11}$$

where the n_m constants σ_k, $k = 1, \ldots, n_m$, associated with the n_m functions $\phi_k(s)$, satisfy the transcendental equation $\cos\sigma_k \cosh\sigma_k = -1$.

Once these constants and functions are defined, the system (6) can be discretized with the standard procedure, giving rise to the following system of nonlinear ODEs

$$\ddot{\mathbf{q}} + (\alpha_0 \mathbf{K} + \beta_0)\dot{\mathbf{q}} + (\mathbf{K} + \mu \mathbf{H})\mathbf{q} = \mathbf{N}(\mathbf{q}, \dot{\mathbf{q}}, \ddot{\mathbf{q}}) \tag{12}$$

where $\mathbf{q}$ is the $n_m \times 1$ vector collecting the generalized coordinates $q_k(t)$, $\mathbf{K} = \mathrm{diag}(\sigma_k^4)$ is a diagonal matrix, $\mathbf{H}$ is the geometric operator defined by $H_{i,j} = 2\int_0^1 \phi_i \phi_j''\mathrm{d}s$, while $\mathbf{N}(\mathbf{q}, \dot{\mathbf{q}}, \ddot{\mathbf{q}})$ is the nonlinearity vector, whose r-th component is defined as follows

$$N_r(\mathbf{q}, \dot{\mathbf{q}}, \ddot{\mathbf{q}}) = \sum_{h=1}^{5} \sum_{i,j,k}^{n_m} Q_{i,j,k}^{(h)} \Phi_{i,j,k,r}^{(h)} \quad \text{with} \quad r = 1, \ldots, n_m \tag{13}$$

being

$$\begin{aligned} Q_{i,j,k}^{(1)} &= q_i q_j q_k + \alpha_0 (q_i q_j q_k)^{\cdot}, \\ Q_{i,j,k}^{(2)} &= q_k (q_i q_j)^{\cdot}, \\ Q_{i,j,k}^{(3)} &= \mu q_i q_j q_k, \\ Q_{i,j,k}^{(4)} &= \beta_1 q_i q_j \dot{q}_k, \\ Q_{i,j,k}^{(5)} &= \alpha_1 q_i q_j \dot{q}_k, \end{aligned} \tag{14}$$

and

$$
\begin{aligned}
\Phi^{(1)}_{i,j,k,r} &= \int_0^1 (\phi_i'(\phi_j'\phi_k''))'\phi_r \mathrm{d}s,\\
\Phi^{(2)}_{i,j,k,r} &= -\tfrac{1}{2}\int_0^1 \phi_r'\phi_k'(\int_1^s \int_s^{s^*} (\phi_i'\phi_j'))\mathrm{d}s,\\
\Phi^{(3)}_{i,j,k,r} &= 3\int_0^1 (\phi_i'\phi_j'\phi_k''\phi_r)\mathrm{d}s - \phi_{iB}'\phi_{jB}'\int_0^1 \phi_k''\phi_r \mathrm{d}s,\\
\Phi^{(4)}_{i,j,k,r} &= \int_0^1 \phi_i\phi_j\phi_k\phi_r \mathrm{d}s,\\
\Phi^{(5)}_{i,j,k,r} &= \int_0^1 (\phi_i''\phi_j''\phi_k'')''\phi_r \mathrm{d}s.
\end{aligned}
\tag{15}
$$

3. Linear stability analysis

To investigate the system's behavior near a Hopf bifurcation, characterized by the critical load μ_d and the associated oscillation frequency ω_d, a linear stability analysis must first be performed. This section provides only a brief overview of this linear analysis. For a comprehensive treatment of this classical task and its key results, the reader is referred to [21,23,27,30,32,52].

The linear stability analysis of the system requires computing the eigenvalues and eigenvectors of the linearized form of Eq. (12). The analysis is carried out for increasing values of the load parameter μ, starting from zero. Stability is lost when the real part of the first eigenvalue (associated with the lowest frequency) crosses from left to right the vertical axis of the complex plane. This defines a critical load μ_d and a corresponding critical frequency ω_d, both of which depend on the damping parameters. Therefore, the Hopf critical frequency ω_d and the associated critical load μ_d must satisfy the underlying eigenvalue problem

$$
\mathcal{L}\mathbf{U} = 0, \tag{16}
$$

where $\mathcal{L}$ is a linear operator defined as

$$
\mathcal{L} = -\omega_d^2\mathbf{I} + i\omega_d(\alpha_0\mathbf{K} + \beta_0\mathbf{I}) + \mathbf{K} + \mu_d\mathbf{H}, \tag{17}
$$

and $\mathbf{U}$ is the associated eigenvector. For completeness, we also define here the vector $\mathbf{V}$, which represents the eigenvector of the adjoint problem

$$
\mathcal{L}^*\mathbf{V} = 0, \tag{18}
$$

where $\mathcal{L}^*$ denotes the adjoint, i.e., the transpose conjugate, of the operator $\mathcal{L}$. The vector $\mathbf{V}$ plays an important role in the perturbation approach introduced in Sect. 4 to analyze the post-critical behavior of the system under consideration.

A graphical representation of the Hopf critical load μ_d and the associated oscillation frequency ω_d is provided in Fig. 2 as a function of the linear damping parameters α_0 and β_0.

As well-established in the literature, the critical load μ_d exhibits a significant reduction for small values of the internal damping coefficient α_0 compared to the undamped Beck's beam, highlighting its destabilizing effect. Conversely, even small values of the external damping coefficient β_0 tend to stabilize the system. These behaviors are particularly evident when examining cross sections of the surface illustrated in Fig. 2. For a more comprehensive analysis and discussion of the linear stability diagrams for

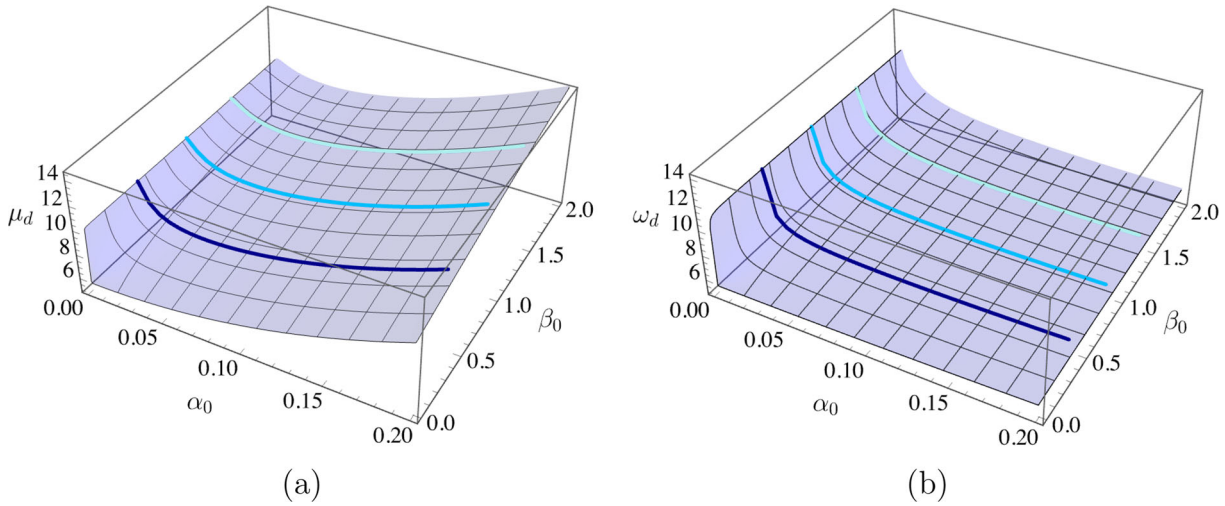

FIG. 2. Three-dimensional representation of the Hopf bifurcation in terms of: **a** critical load μ_d, and **b** associated oscillation frequency ω_d, plotted as functions of the internal and external damping parameters α_0 and β_0. The three lines are taken at $\beta_0 = 0.5$, 1, 2, respectively

the system under investigation, the reader is referred, e.g., to [23,30]. In general, the influence of linear damping on the stability of a generalized Beck's beam can be summarized as follows:

- for a given β_0, a small value of α_0 results in a critical load lower than that of the undamped case, indicating a destabilizing effect;
- the greater the value of β_0, the less pronounced is the destabilizing effect of α_0;
- when α_0 becomes sufficiently large, the destabilizing effect of internal damping tends to vanish;
- for a fixed pair (α_0, β_0), the critical load μ_d increases with β_0, and it may also increase with α_0 if the latter is sufficiently large.

In the following, the nonlinear analysis is carried out starting from selected values of damping coefficients α_0 and β_0, with particular focus on the parameter region where the damping-induced destabilization is observed.

4. Multiple scale analysis

The discretized problem under consideration is analyzed in this section using a perturbation approach based on the Multiple Scales Method (MSM). Introducing a small positive scaling parameter $\epsilon \ll 1$, multiple time scales are defined as $t_0 = t$, $t_1 = \epsilon t$, and $t_2 = \epsilon^2 t$. Correspondingly, the discrete variables are expanded in powers of ϵ as follows:

$$\mathbf{q}(t) = \epsilon^{1/2}\mathbf{q}_0(t_0, t_1, t_2) + \epsilon\mathbf{q}_1(t_0, t_1, t_2) + \epsilon^{3/2}\mathbf{q}_2(t_0, t_1, t_2) \tag{19}$$

The perturbation strategy is developed to analyze the system's behavior as the load parameter μ varies within a small neighborhood of the Hopf critical value μ_d (subscript d denotes *damped* case). To this end, the change of variable $\mu = \mu_d + \epsilon\delta\mu$ is introduced, where $\delta\mu$ represents the load increment from the Hopf bifurcation point. With this formulation, the discretized system of nonlinear ODEs can be cast into the following hierarchy:

$$\epsilon^0: \quad \ddot{\mathbf{q}}_0 + (\alpha_0\mathbf{K} + \beta_0)\dot{\mathbf{q}}_0 + (\mathbf{K} + \mu_d\mathbf{H})\mathbf{q}_0 = \mathbf{0} \tag{20}$$

$$\epsilon^1: \quad \ddot{\mathbf{q}}_1 + (\alpha_0\mathbf{K} + \beta_0)\dot{\mathbf{q}}_1 + (\mathbf{K} + \mu_d\mathbf{H})\mathbf{q}_1 = \mathbf{N}_1(\delta\mu, \alpha_1, \beta_1, \mathbf{q}_0) \tag{21}$$

$$\epsilon^2: \quad \ddot{\mathbf{q}}_2 + (\alpha_0\mathbf{K} + \beta_0)\dot{\mathbf{q}}_2 + (\mathbf{K} + \mu_d\mathbf{H})\mathbf{q}_2 = \mathbf{N}_2(\delta\mu, \alpha_1, \beta_1, \mathbf{q}_0, \mathbf{q}_1) \tag{22}$$

The solution of the ϵ^0-order problem reads

$$\mathbf{q}_0 = \mathbf{U}A(t_1, t_2)e^{i\omega_d t} + cc \tag{23}$$

where ω_d is the critical frequency corresponding to the Hopf critical load μ_d, $\mathbf{U}$ is the associated eigenvector defined through Eq. (16), and $A(t_1, t_2)$ is the unknown amplitude to be determined by solving the higher order problems.

Given μ_d and ω_d, the solutions of the linear problem (20) is known and can be substituted in the forcing term of the ϵ^1 problem. This latter contains secular terms that must be removed by imposing the solvability condition [50]

$$\int_0^{2\pi/\omega_d} \mathbf{V} \cdot \mathbf{N}_1(\delta\mu, \alpha_1, \beta_1, \mathbf{q}_1)e^{-i\omega_d t_0}\mathrm{d}t_0 = 0, \tag{24}$$

where $\mathbf{V}$ represents the left eigenvector of the adjoint problem (18). By solving the latter expression for $\partial_{t_1}A(t_1, t_2)$, it is possible to derive the modulation equations at the first nonlinear order in complex form

$$\begin{aligned} \partial_{t_1}A(t_1, t_2) &= \varrho_1\delta\mu\, A + (\alpha_1\varrho_2 + \beta_1\varrho_3 + \varrho_4)A^2\bar{A}, \\ \partial_{t_1}\bar{A}(t_1, t_2) &= \bar{\varrho}_1\delta\mu\, \bar{A} + (\alpha_1\bar{\varrho}_2 + \beta_1\bar{\varrho}_3 + \bar{\varrho}_4)A\bar{A}^2. \end{aligned} \tag{25}$$

Note that the coefficients appearing in the latter expression are functions of the linear parameters (α_0, β_0) and (μ_d, ω_d). The so defined amplitude modulation equations (AME) allow to eliminate the resonant terms from the right end side of the ϵ^1-order problem that becomes then solvable and its solution assumes the expression

$$\mathbf{q}_1 = \gamma_1 A^3(t_1, t_2)e^{3i\omega_d t_0} + \gamma_2 A^2(t_1, t_2)\bar{A}(t_1, t_2)e^{i\omega_d t_0} + \gamma_3\delta\mu A(t_1, t_2)e^{i\omega_d t_0} + cc. \tag{26}$$

Note that the vectors $\gamma_{1,2,3}$ are functions of the linear parameters (α_0, β_0) and (μ_d, ω_d), while only γ_1 also depends on the nonlinear damping parameters (α_1, β_1). Such vectors are derived by solving separately the following algebraic problems:

$$\begin{aligned} \left[-9\omega_d^2\mathbf{I} + i\omega_d(\alpha_0\mathbf{K} + \beta_0) + (\mathbf{K} + \mu_d\mathbf{H})\right]\gamma_1 &= \mathbf{z}_1 A^3(t_1, t_2), \\ \left[-\omega_d^2\mathbf{I} + i\omega_d(\alpha_0\mathbf{K} + \beta_0) + (\mathbf{K} + \mu_d\mathbf{H})\right]\gamma_2 &= \mathbf{z}_2 A^2(t_1, t_2)\bar{A}(t_1, t_2), \\ \left[-\omega_d^2\mathbf{I} + i\omega_d(\alpha_0\mathbf{K} + \beta_0) + (\mathbf{K} + \mu_d\mathbf{H})\right]\gamma_3 &= \mathbf{z}_3\delta\mu A(t_1, t_2). \end{aligned} \tag{27}$$

Specifically, γ_1 is obtained by solving a non-singular problem, whereas determining $\gamma_{2,3}$ involves solving singular problems. The procedure closely follows that outlined in [21], to which the reader is referred for additional details.

Given $\mathbf{q}_1$, the solvability condition can be imposed at order ϵ^2 to derive a correction to the amplitude modulation equations. The condition is again

$$\int_0^{2\pi/\omega_d} \mathbf{V}\cdot\mathbf{N}_2(\delta\mu,\alpha_1,\beta_1,\mathbf{q}_1)e^{-i\omega_d t_0}\mathrm{d}t_0 = 0, \tag{28}$$

from which the second-order AMEs are derived.

$$\begin{aligned}\partial_{t_2}A(t_1,t_2) =& A\delta\mu^2\varrho_5 + A^2\bar{A}\left(\alpha_1\delta\mu\varrho_6+\beta_1\delta\mu\varrho_7+\delta\mu\varrho_8\right)+\\ & A^3\bar{A}^2\left(\alpha_1\beta_1\varrho_{10}+\alpha_1^2\varrho_9+\alpha_1\varrho_{11}+\beta_1^2\varrho_{12}+\beta_1\varrho_{13}+\varrho_{14}\right),\\ \partial_{t_2}\bar{A}(t_1,t_2) =& \delta\mu^2\bar{A}\bar{\varrho}_5 + A\bar{A}^2\left(\alpha_1\delta\mu\bar{\varrho}_6+\beta_1\delta\mu\bar{\varrho}_7+\delta\mu\bar{\varrho}_8\right)+\\ & A^2\bar{A}^3\left(\alpha_1\beta_1\bar{\varrho}_{10}+\alpha_1^2\bar{\varrho}_9+\alpha_1\bar{\varrho}_{11}+\beta_1^2\bar{\varrho}_{12}+\beta_1\bar{\varrho}_{13}+\bar{\varrho}_{14}\right).\end{aligned} \tag{29}$$

The amplitude modulation equations can be cast in real form by introducing $A(t_1,t_2) = (1/2)a(t_1,t_2)e^{i\varphi(t_1,t_2)}$, being a and φ the real amplitude and phase, respectively, that is

$$\begin{aligned}\dot{a} =& \delta\mu\left(a\varrho_1+\frac{a^3\varrho_5}{4}\right)+\frac{1}{4}a^3(\alpha_1\varrho_2+\beta_1\varrho_3+\varrho_4)+\frac{1}{16}a^5(\alpha_1\varrho_6+\beta_1\varrho_7+\varrho_8),\\ a\dot{\varphi} =& \delta\mu\left(a\bar{\varrho}_1+\frac{a^3\bar{\varrho}_5}{4}\right)+\frac{1}{4}a^3(\alpha_1\bar{\varrho}_2+\beta_1\bar{\varrho}_3+\bar{\varrho}_4)+\frac{1}{16}a^5(\alpha_1\bar{\varrho}_6+\beta_1\bar{\varrho}_7+\bar{\varrho}_8).\end{aligned} \tag{30}$$

Note that the coefficients appearing in the latter expressions represent the real part of the ones appearing in Eqs. (25),(29), while those denoted by the over bar represent the imaginary part.

The interest is to analyze the stationary solutions of Eq. (30) when $\dot{a} = 0$, therefore, for a given value of a only one corresponding value of $\delta\mu$ can exist, that is

$$\delta\mu = -\frac{a^2\left(\alpha_1\varrho_2+\beta_1\varrho_3+\varrho_4\right)+\frac{1}{4}a^4\left(\alpha_1\varrho_6+\beta_1\varrho_7+\varrho_8\right)}{a^2\varrho_5+4\varrho_1}, \tag{31}$$

which allows to depict the bifurcation diagram of the system, i.e., to describe its Limit Cycle Oscillation (LCO) in the plane ($\delta\mu$, a). In particular, with regard to the numerical results, the response will always be represented in terms of the beam displacement at the tip, i.e., $v(1)$.

The stability of the obtained solution can be analyzed by linearizing Eq.(30), yielding the following expression:

$$5\alpha_1a^4\varrho_6+5a^4\beta_1\varrho_7+5a^4\varrho_8+12\alpha_1a^2\varrho_2+12a^2\beta_1\varrho_3+12a^2\delta\mu\varrho_5+12a^2\varrho_4+16\delta\mu\varrho_1 = 0. \tag{32}$$

This expression must be evaluated along the limit cycle at the corresponding values of $\delta\mu$ and a; when it takes positive values, the solution is unstable.

5. Numerical examples

5.1. Role played by nonlinear damping coefficients α_1 and β_1

When the solutions experiences a transitions from a subcritical to a supercritical branch of the amplitude-load stability diagram, a turning point appears in the LCO, as depicted in Fig. 3.

The amplitude at which it occurs can be evaluated as $\partial\delta\mu/\partial a = 0$, which furnishes a biquadratic polynomial in the real amplitude a, i.e.,

$$b_2(a^2)^2+b_1a^2+b_0 = 0, \tag{33}$$

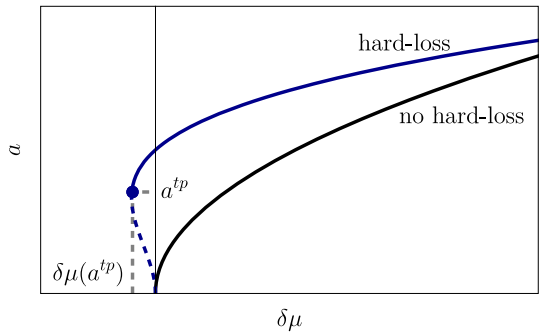

FIG. 3. Qualitative representation of the Limit Cycle Oscillation (LCO) in the absence (black line) and in the presence of hard loss

whose solutions are

$$a_{1,2}^{tp} = \sqrt{\frac{-b_1 + \sqrt{\Delta}}{2b_2}}, \tag{34}$$

where the superscript tp stands for turning point, $\Delta = b_1^2 - 4b_0b_2$, the corresponding $\delta\mu$ is given by Eq. (31), and, finally,

$$\begin{aligned} b_0 &= -16\varrho_1\left(\alpha_1\varrho_2 + \beta_1\varrho_3 + \varrho_4\right), \\ b_1 &= -8\varrho_1\left(\alpha_1\varrho_6 + \beta_1\varrho_7 + \varrho_8\right), \\ b_2 &= -\varrho_5\left(\alpha_1\varrho_6 + \beta_1\varrho_7 + \varrho_8\right). \end{aligned} \tag{35}$$

The existence of the turning point can be determined by studying the sign of b_0. In particular, $\Delta > 0$ ensures the existence of two solutions for Eq. (33), but, in order to obtain real a_{tp}, it must be $b_0 < 0$. This coefficient is not only a direct function of (α_1, β_1), but also depends on the linear damping (α_0, β_0) through the coefficients ρ_k.

Figure 4a represents the domain where the turning point exists ($b_0 < 0$) for different values (α_0, β_0). The domain actually represents the region where a_1 is positive from $b_0 < 0$, having imposed $\beta_1 = 0$, since, as it will be clarified next, it has a smaller effect. The domain $\alpha_1 > 0$ is enclosed by the thin red line and highlighted in light blue. The turning point always exists for small values of α_1, however, by looking at the inset in Fig. 4a, it can be noted that there is a smaller region where the turning point does not exists for really small values of α_0, but $\beta_0 > 0.7$. By focusing the attention on smaller values of α_0, namely 0.01 (see the dashed gray line), the condition $b_0 = 0$ is reported in Fig. 4b for $\beta_0 = 0.5, 1, 1.5$, in particular $b_0 < 0$ on the right side. Here, it is possible to highlight that the role of β_1 is marginal unless really large values (unfeasible) are considered. On the other hand, the role of α_1 reveals to be crucial in the existence of the turning point.

Once the a_{tp} is found, the corresponding $\delta\mu$ is retrieved by substituting the amplitude into Eq. (31).

5.2. Limit cycles of the nonlinearly damped system

Equation (31) allows to retrieve the corresponding amplitude in terms of tip displacement $v(1)$. It is clear from the previous analysis that the role of β_1 is marginal since it becomes effective only at large values, i.e., $\beta_1 > 1$, therefore in the subsequent analyses it is fixed at $\beta_1 = 0.005$. On the other hand, it is of

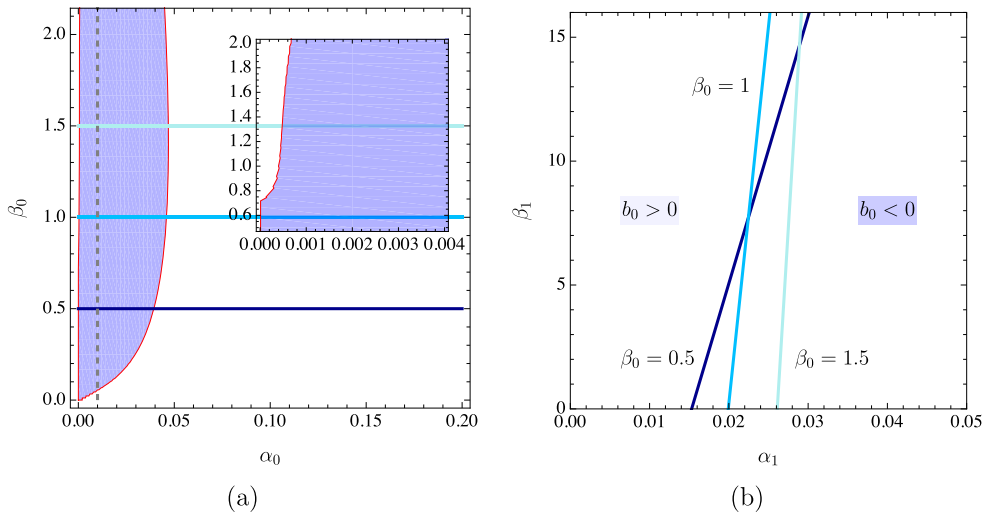

FIG. 4. Existence of the turning point: $b_0(\alpha_1, \beta_1) \geq 0$. **a** The colored region identifies the domain where the turning point exists for different values (α_0, β_0). **b** The existence condition is evaluated at $\alpha_0 = 0.01$ and three selected values of β_0, namely (0.5, 1, 1.5) (colour figure online)

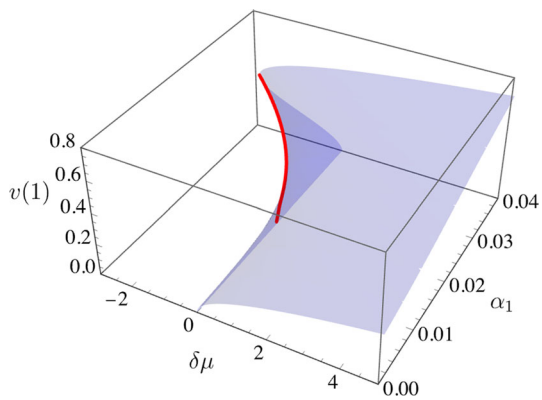

FIG. 5. Limit cycle oscillation amplitude at $\beta_1 = 0.005$.

interest to analyze the response of the solution when α_1 varies: it has been observed that its value can determine a significant variation in the solution stability.

Figure 5 illustrates the LCO amplitude $v(1)$ and the corresponding $\delta\mu$, as α_1 varies in the range $(0, 0.04)$. The light blue surface identifies the amplitude, while the red line indicates the turning point loci.

Figure 6 illustrates three slices of Fig. 5 at prescribed α_1, namely, (0.015, 0.025, 0.027). The perturbation solution is represented in blue (the dashed line denotes the unstable branches) and the blue dot represents the position of the turning point, which exists only in Fig. 6b, c. In all the three subfigures, it is represented the numerical solution (red dotted line) to show the good agreement with the analytical one, even at significant amplitudes, i.e., $v(1) \simeq 0.4$.

To better highlight the good agreement with the numerical solution, also the response in terms of phase diagrams is reported in Fig. 5 (perturbation solution in blue and the numerical one in red) at

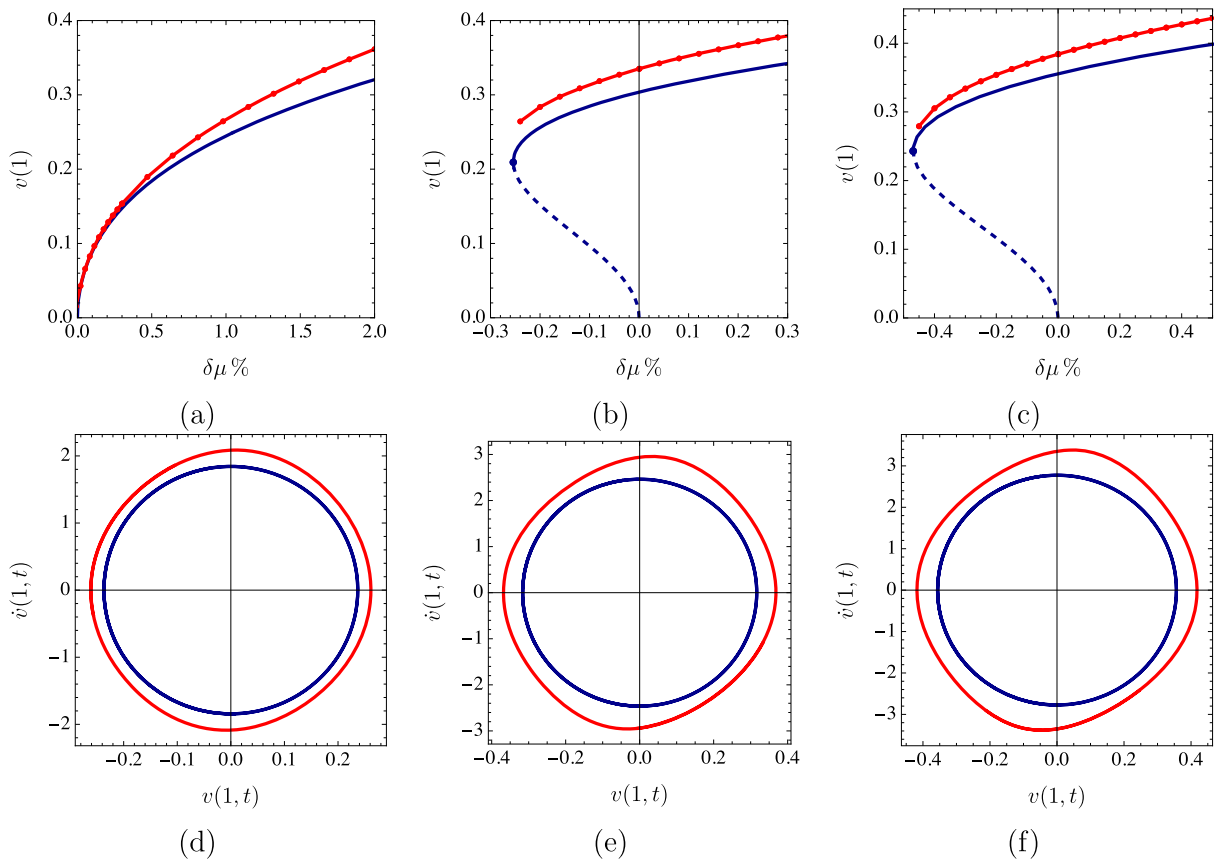

FIG. 6. Limit cycle oscillation amplitude at $\beta_1 = 0.005$ and: **a** $\alpha_1 = 0.015$; **b** $\alpha_1 = 0.025$; **c** $\alpha_1 = 0.027$. The corresponding phase diagram is taken at: **d** $\delta\mu = 1\%$ for $\alpha_1 = 0.015$; **e** $\delta\mu = 0.2\%$ for $\alpha_1 = 0.025$; **f** $\delta\mu = 0.3\%$ for $\alpha_1 = 0.027$.

selected values of $\delta\mu$, namely : (d) $\delta\mu = 1\%$ for $\alpha_1 = 0.015$; (e) $\delta\mu = 0.2\%$ for $\alpha_1 = 0.025$; (f) $\delta\mu = 0.3\%$ for $\alpha_1 = 0.027$. Despite a quantitative mismatch is present, the overall response is well captured event at large amplitudes (i.e., $v(1) > 0.3$).

6. Conclusions

The impact of various nonlinear damping sources, arising from material behavior (internal damping) and fluid–structure interaction (external damping), on the nonlinear dynamics of a Beck's beam has been analytically investigated. A perturbation analysis based on the Multiple Scales Method has been employed to derive the system's bifurcation equation near a Hopf bifurcation and to assess the role of nonlinear damping in shaping the system's nonlinear response. The analytical investigation has revealed that both internal and external damping mechanisms can have a dual effect: they may either attenuate or amplify the amplitude of the system's limit cycles and, under specific conditions, can induce a transition from stable supercritical to unstable subcritical limit cycles. Specifically, the analysis has revealed the presence of a turning point in the amplitude-load curve, along with the condition for its occurrence, which marks a regain of stability in the subcritical branch. Beyond the turning point, the subcritical branch transitions into a supercritical type, causing a reversal in the nature of the limit cycle. This

phenomenon, known as Hard Loss of Stability and previously identified analytically only in the context of the Ziegler's double pendulum, has now also been observed and analytically demonstrated in the Beck's beam. Numerical analysis and comparisons between the analytical solution obtained via the MSM and the numerical solution derived using the Galerkin method, have further validated these analytical findings.

The study has revealed damping effects in the nonlinear regime that extend beyond the classical destabilization phenomena observed in linear systems. The damping-induced stabilization and destabilization behaviors, along with the analytical conditions under which they arise, identified in this work, offer valuable insights that could be harnessed in the design of advanced mechanical systems. These findings hold potential for applications across a range of engineering fields, including energy harvesting and vibration control.

Several aspects deserve further investigation, including the coupling of the considered nonlinear viscoelastic beam with piezoelectric materials [43,47], as well as the use of alternative beam geometries, such as tapered, pre-twisted, or curved configurations [53,54], to optimize the system's response for energy harvesting applications. The influence of piezoelectric patches on nonlinear viscoelastic non-prismatic elements, both for energy harvesting and vibration control, represents an intriguing area for future research.

Acknowledgements

Author contributions G.M. and A.C.: Writing—original draft, Writing—review & editing, Methodology, Investigation, Formal analysis. F.D.: Writing—review & editing, Methodology, Conceptualization, Supervision.

Funding Open access funding provided by Università degli Studi dell'Aquila within the CRUI-CARE Agreement.

Data availability No datasets were generated or analyzed during the current study.

Declarations
Conflict of interest The authors declare no Conflict of interest.

Appendix A Extended Hamilton's principle and governing equations

The equations of motion of the system presented in Sect. 2 are derived using the extended Hamilton's principle, which states that the variational condition $\delta\mathcal{H} := \delta\mathcal{T} + \delta\mathcal{W}_e - \delta\mathcal{W}_i = 0$ must be satisfied for any kinematically admissible motion of the system over an arbitrary time interval $[t_1, t_2]$, where $\delta\mathcal{T}$ is the kinetic energy of the system, $\delta\mathcal{W}_e$ is the external work, and $\delta\mathcal{W}_i$ is the internal work. They are defined

as follows:

$$\delta\mathcal{T} := \delta \int_{t_1}^{t_2} \int_{0}^{l} m \, \frac{\dot{u}^2 + \dot{v}^2}{2} \, \mathrm{d}s\mathrm{d}t, \tag{36}$$

$$\delta\mathcal{W}_e := \int_{t_1}^{t_2} \int_{0}^{l} p \, \delta v \, \mathrm{d}s\mathrm{d}t + \int_{t_1}^{t_2} \Big((-F\cos\theta_B)\, \delta u_B + (-F\sin\theta_B)\, \delta v_B \Big) \mathrm{d}t, \tag{37}$$

$$\delta\mathcal{W}_i := \int_{t_1}^{t_2} \int_{0}^{l} M \, \delta\kappa \, \mathrm{d}s\mathrm{d}t + \delta \int_{t_1}^{t_2} \int_{0}^{l} \Big(H\,(u' - \cos\theta + 1) + V\,(v' - \sin\theta) \Big) \mathrm{d}s\mathrm{d}t. \tag{38}$$

The kinematic constraints associated with beam inextensibility and unshearability are incorporated into Eq. (38) through Lagrange multipliers $H(s,t)$ and $V(s,t)$, which represent the reactive internal forces in the horizontal and vertical directions, respectively.

By applying standard procedures based on integration by parts and the principle of localization, the equations of motion of the system can be expressed in the form:

$$\begin{aligned} &H'(s,t) - m\,\ddot{u}(s,t) = 0, \\ &V'(s,t) + p(s,t) - m\,\ddot{v}(s,t) = 0, \\ &M'(s,t) - H(s,t)\sin\theta(s,t) + V(s,t)\cos\theta(s,t) = 0, \end{aligned} \tag{39}$$

with the *constraint* equations $v'(s,t) = \sin\theta(s,t)$ and $u'(s,t) = \cos\theta(s,t) - 1$, the *geometric* boundary conditions $v(0,t) = 0$ and $v'(0,t) = 0$, and the *natural* boundary conditions

$$\begin{aligned} &H(l,t) + F\cos\theta(l,t) = 0, \\ &V(l,t) + F\sin\theta(l,t) = 0, \\ &M(l,t) = 0. \end{aligned} \tag{40}$$

Equations (39)–(40) can be combined and reformulated as an integro-differential problem in terms of a single unknown function, $v(s,t)$. Specifically, this leads to the integro-differential equation (1), coupled with four boundary conditions: $v(0,t) = 0$, $v'(0,t) = 0$, $M(l,t) = 0$, and $M'(l,t) = 0$. Here, the internal bending moment $M(s,t)$ is explicitly expressed as a function of $v(s,t)$ through the constitutive relation given in Eq. (2).

References

[1] Koiter, W.: Elastic Stability of Solids and Structures. Cambridge University Press, Cambridge (2009)
[2] Timoshenko, S., Gere, J.: Theory of Elastic Stability. Dover Publications, New York (2009)
[3] Pignataro, M., Rizzi, N., Luongo, A.: Stability, Bifurcation and Postcritical Behaviour of Elastic Structures. Elsevier, New York (1991)
[4] Beck, M.: Die knicklast des einseitig eingespannten, tangential gedrückten stabes. Z. Angew. Math. Phys. **3**(3), 225–228 (1952)
[5] Ziegler, H.: Die stabilitätskriterien der elastomechanik. Ingenieur-Archiv **20**(1), 49–56 (1952)
[6] Langthjem, M., Sugiyama, Y.: Dynamic stability of columns subjected to follower loads: a survey. J. Sound Vib. **238**(5), 809–851 (2000)
[7] Ryu, B., Katayama, K., Sugiyama, Y.: Dynamic stability of Timoshenko columns subjected to subtangential forces. Comput. Struct. **68**, 499–512 (1998)
[8] Fazelzadeh, S., Mazidi, A.: Nonlinear aeroelastic analysis of bending-torsion wings subjected to a transverse follower force. J. Comput. Nonlinear Dyn. **6**(3), 031016 (2011)

[9] Datta, P., Biswas, S.: Aeroelastic behavior of aerospace structural elements with follower force: a review. Int. J. Aeronaut. Space Sci. **12**(2), 134–148 (2011)
[10] Bigoni, D., Noselli, G.: Experimental evidence of flutter and divergence instabilities induced by dry friction. J. Mech. Phys. Solids **59**(10), 2208–2226 (2011)
[11] Bennati, S., Barsotti, R., Migliaccio, G.: A simple model for predicting the nonlinear dynamic behavior of elastic systems subjected to friction. In: Carcaterra, A., Paolone, A., Graziani, G. (eds.) Proceedings of XXIV AIMETA Conference 2019, pp. 1415–1425. Springer, Cham (2020)
[12] Barsotti, R., Bennati, S., Migliaccio, G.: Non-linear dynamics of simple elastic systems undergoing friction-ruled stick–slip motions. CivilEng **5**, 420–434 (2024)
[13] Wang, L.: Flutter instability of supported piped conveying fluid subjected to distributed follower forces. Acta. Mech. Sin. **25**, 46–52 (2012)
[14] Tsiatas, G., Katsikadelis, J.: Post-critical behavior of damped beam columns with variable cross section subjected to distributed follower forces. Nonlinear Dyn. **56**, 429–441 (2008)
[15] Blevins, R.: Flow-Induced Vibration. Van Nostrand Reinhold, New York (1990)
[16] Bhovad, P., Kaufmann, J., Li, S.: Peristaltic locomotion without digital controllers: exploiting multi-stability in origami to coordinate robotic motion. Extreme Mech. Lett. **32**, 100552 (2009)
[17] Fazelzadeh, S., Eghtesad, M., Azadi, M.: Buckling and flutter of a column enhanced by piezoelectric layers and lumped mass under a follower force. Int. J. Struct. Stab. Dyn. **10**, 1083–1097 (2010)
[18] D'Annibale, F., Rosi, G., Luongo, A.: Piezoelectric control of Hopf bifurcations: a non-linear discrete case study. Int. J. Non-Linear Mech. **80**, 160–169 (2016)
[19] Bigoni, D., Dal Corso, F., ON, K., Misseroni, D., Noselli, G., Piccolroaz, A.: Flutter instability in solids and structures, with a view on biomechanics and metamaterials. Proc. R. Soc. A **479**, 20230523 (2023)
[20] Luongo, A., D'Annibale, F.: A paradigmatic minimal system to explain the Ziegler paradox. Continuum Mech. Thermodyn. **27**, 211–222 (2015)
[21] Luongo, A., D'Annibale, F., Ferretti, M.: Hard loss of stability of Ziegler's column with nonlinear damping. Meccanica **51**, 2647–2663 (2016)
[22] Luongo, A., D'Annibale, F.: Nonlinear hysteretic damping effects on the post-critical behaviour of the visco-elastic Beck's beam. Math. Mech. Solids **22**(6), 1347–1365 (2017)
[23] Migliaccio, G., D'Annibale, F.: On the role of different nonlinear damping forms in the dynamic behavior of the generalized Beck's column. Nonlinear Dyn. **112**, 13733–13750 (2024)
[24] Langthjem, M., Sugiyama, Y.: Optimum design of cantilevered columns under the combined action of conservative and nonconservative loads, part i: the undamped case. Comput. Struct. **74**, 385–398 (2000)
[25] Migliaccio, G., D'Annibale, F., Koutsogiannakis, P., Dal Corso, F.: Viscous damping stabilization and destabilization of resonant self-tuning variable-length structures. Eur. J. Mech. A. Solids **114**, 105727 (2025)
[26] Seyranian, A., Mailybaev, A.: Multiparameter Stability Theory with Mechanical Applications, vol. 13. World Scientific, Singapore (2003)
[27] Kirillov, O.: A theory of the destabilization paradox in non-conservative systems. Acta Mech. **174**, 145–166 (2005)
[28] Luongo, A., Ferretti, M., D'Annibale, F.: Paradoxes in dynamic stability of mechanical systems: investigating the causes and detecting the nonlinear behaviors. Springerplus **5**(1), 60 (2016)
[29] Kirillov, O., Seyranian, A.: The effect of small internal and external damping on the stability of distributed non-conservative systems. J. Appl. Math. Mech. **69**(4), 529–552 (2005)
[30] Luongo, A., D'Annibale, F.: Double zero bifurcation of non-linear viscoelastic beams under conservative and non-conservative loads. Int. J. Non-Linear Mech. **55**, 128–139 (2013)
[31] Detinko, F.: Lumped damping and stability of Beck column with a tip mass. Int. J. Solids Struct. **40**(17), 4479–4486 (2003)
[32] Luongo, A., D'Annibale, F.: On the destabilizing effect of damping on discrete and continuous circulatory systems. J. Sound Vib. **133**, 6723–6741 (2014)
[33] Kirillov, O.: Non Conservative Stability Problems of Modern Physics. De Gruyter, Berlin (2013)
[34] Elishakoff, I.: Controversy associated with the so-called "follower forces": critical overview. Appl. Mech. Rev. **58**(2), 117–142 (2005)
[35] D'Annibale, F., Ferretti, M.: On the effects of linear damping on the nonlinear Ziegler's column. Nonlinear Dyn. **103**(4), 3149–3164 (2021)
[36] Crespo da Silva, M.: Harmonic non-linear response of Beck's column to a lateral excitation. Int. J. Solids Struct. **14**(12), 987–997 (1978)
[37] Crespo da Silva, M.: Flexural-flexural oscillations of Beck's column subjected to a planar harmonic excitation. J. Sound Vib. **60**(1), 133–144 (1978)
[38] Tomski, L., Szmidla, J., Uzny, S.: The local and global instability and vibration of systems subjected to non-conservative loading. Thin-Walled Struct. **45**, 945–949 (2007)

[39] Uzny, S., Sokól, K., Warys, P.: Flutter and divergence instability regions of a column subjected to the load realized by means of a jet engine with an additional guiding structure. J. Sound Vib. **549**, 117580 (2023)
[40] Bigoni, D., Kirillov, O., Misseroni, D., Noselli, G., Tommasini, M.: Flutter and divergence instability in the Pflüger column: experimental evidence of the Ziegler destabilization paradox. J. Mech. Phys. Solids **116**, 99–116 (2018)
[41] Bigoni, D., Misseroni, D.: Structures loaded with a force acting along a fixed straight line, or the "Reut's column problem". J. Mech. Phys. Solids **134**, 103741 (2020)
[42] Di Egidio, A., Luongo, A., Paolone, A.: Linear and non-linear interactions between static and dynamic bifurcations of damped planar beams. Int. J. Non-Linear Mech. **42**(1), 88–98 (2007)
[43] Casalotti, A., D'Annibale, F.: A rod-like piezoelectric controller for the improvement of the visco-elastic Beck's beam linear stability. Struct. Control. Health Monit. **29**, 1–15 (2021)
[44] D'Annibale, F., Rosi, G., Luongo, A.: On the failure of the 'similar piezoelectric control' in preventing loss of stability by nonconservative positional forces. Z. Angew. Math. Phys. **66**(4), 1949–1968 (2015)
[45] Casalotti, A., D'Annibale, F.: Improving the linear stability of the visco-elastic Beck's beam via piezoelectric controllers. J. Appl. Comput. Mech. **7**(Special Issue), 1098–1109 (2021)
[46] Casalotti, A., D'Annibale, F.: On the effectiveness of a rod-like distributed piezoelectric controller in preventing the Hopf bifurcation of the visco-elastic Beck's beam. Acta Mech. **233**, 1819–1836 (2022)
[47] Casalotti, A., D'Annibale, F.: On the effects of a beam-like piezoelectric passive controller on the linear stability of the visco-elastic Beck's beam. Mech. Res. Commun. **125**, 103980 (2022)
[48] Duncan, W.: Galerkin's method in mechanics and differential equations, Aeronautical Research Committee Reports and Memoranda 1798 (1937)
[49] Finlayson, B., Scriven, L.: The method of weighted residuals—a review. Appl. Mech. Rev. **19**(9), 735–748 (1966)
[50] Nayfeh, A., Mook, D.: Nonlinear oscillations. Wiley-VCH Verlag GmbH & Co. KGaA, Weinheim (2004) (First published: 26 May 1995)
[51] Nayfeh, A.: Perturbation methods. Wiley-VCH Verlag GmbH & Co. KGaA, Weinheim (2004) (First published: 15 August 2000)
[52] Langthjem, M., Sugiyama, Y.: Optimum design of cantilevered columns under the combined action of conservative and nonconservative loads, part ii: the damped case. Comput. Struct. **74**, 399–408 (2000)
[53] Migliaccio, G., Ruta, G.: The influence of an initial twisting on tapered beams undergoing large displacements. Meccanica **56**(7), 1831–1845 (2021)
[54] Migliaccio, G., D'Annibale, F.: On the inadequacy of a stepped-beam approach in predicting shear stresses in tapered slender solids. Eur. J. Mech. A. Solids **111**, 105590 (2025)

G. Migliaccio and F. D'Annibale
Department of Civil, Construction-Architectural and Environmental Engineering
University of L'Aquila
67100 L'Aquila
Italy
e-mail: francesco.dannibale@univaq.it

A. Casalotti
Department of Architecture
University of Roma Tre
00185 Rome
Italy

(Received: July 31, 2025; revised: September 17, 2025; accepted: September 22, 2025)